Received February 18, 2019, accepted February 25, 2019, date of publication March 4, 2019, date of current version March 25, 2019.

Digital Object Identifier 10.1109/ACCESS.2019.2902718

An Energy-Efficient Algorithm for Classification of Fall Types Using a Wearable Sensor

SOON BIN KWON[1], JEONG-HO PARK[2], CHIHEON KWON[3], HYUNG JOONG KONG[4], JAE YOUN HWANG[2], AND HEE CHAN KIM[1,3,5], (Member, IEEE)

[1]Interdisciplinary Program in Bioengineering, Seoul National University, Seoul 03080, South Korea
[2]Department of Information and Communication Engineering, Daegu Gyeongbuk Institute of Science and Technology, Daegu 42988, South Korea
[3]Medical Research Center, Department of Biomedical Engineering, College of Medicine, Seoul National University, Seoul 03080, South Korea
[4]Department of Biomedical Engineering, College of Medicine, Chungnam National University, Daejeon 35015, South Korea
[5]Department of Biomedical Engineering, College of Medicine, Seoul National University, Seoul 03080, South Korea

Corresponding author: Hee Chan Kim (hckim@snu.ac.kr)

This work was supported in part by the Korean Government (MSIP and MOHW), through the Bio and Medical Technology Development Program of the National Research Foundation, under Grant 2016M3A9F1939646.

ABSTRACT Objective: To mitigate damage from falls, it is essential to provide medical attention expeditiously. Many previous studies have focused on detecting falls and have shown that falls can be accurately detected at least in a laboratory setting. However, a very few studies have classified the different types of falls. To this end, in this paper, a novel energy-efficient algorithm that can discriminate the five most common fall types was developed for wearable systems. Methods: A wearable system with an inertial measurement unit sensor was first developed. Then, our novel algorithm, temporal signal angle measurement (TSAM), was used to classify the different types of falls at various sampling frequencies, and the results were compared with those from three different machine learning algorithms. Results: The overall performance of the TSAM and that of the machine learning algorithms were similar. However, the TSAM outperformed the machine learning algorithms at frequencies in the range of 10–20 Hz. As the sampling frequency dropped from 200 to 10Hz, the accuracy of the TSAM ranged from 93.3% to 91.8%. The sensitivity and specificity ranges from 93.3% to 91.8%, and 98.3% to 97.9%, respectively for the same frequency range. Conclusion: Our algorithm can be utilized with energy-efficient wearable devices at low sampling frequencies to classify different types of falls. Significance: Our system can expedite medical assistance in emergency situations caused by falls by providing the necessary information to medical doctors or clinicians.

INDEX TERMS Fall detection, fall type classification, machine learning, temporal signal angle measurement, wearable device.

I. INTRODUCTION

Falls constitute a major problem owing to aging populations worldwide. It is known that one-third of the elderly population aged 65 or above experience falls at least once per year [1]. Additionally, falls are a crucial issue with people who are in specialized professions such as firefighters or construction workers [2], [3]. For these groups of people, falls could lead to serious injuries, such as bone fractures or head traumas or secondary damage. To reduce damage, it is important to detect and rescue these people in a timely manner as individuals left unattended after a fall are exposed to high risks. Thus, it is important to develop a system capable of automatically detecting falls.

Previous studies have developed a variety of fall detection systems based on optical sensors [4]–[12], accelerometers [13]–[18], and inertial measurement units (IMUs) [2], [19]–[21]. Fall detection based on optical sensors, including traditional cameras and depth image sensors, is the most commonly used technique at present. In this fall detection technique, humans are distinguished from the images acquired by the optical sensor, and a classification algorithm is then applied to detect the fall. Yu *et al.* developed a fall detection system using a traditional camera [9]. They extracted ellipses and shape-structure features from the image captured and applied an one-class support vector machine to classify the fall. Rougier *et al*. also used images captured

The associate editor coordinating the review of this manuscript and approving it for publication was Gang Mei.

using a camera to detect falls [6]. Their method utilizes shape analysis to calculate the deformation of the silhouettes, and a Gaussian mixture model to detect the fall. A frequently used depth image sensor to detect falls is Microsoft Kinect. Stone *et al*. characterized the in-depth image of an individual's vertical state captured using Kinect and classified the fall based on an ensemble of the decision tree [7]. Mastorakis *et al*. also used data collected using Kinect to detect falls [22]. However, even though fall detection systems based on optical sensors provide accurate results, they have a limited and fixed range of detection. Additionally, there are privacy concerns when using such visual methods.

A wearable sensor based on accelerometers or IMU sensors does not have any privacy issues and also is not limited to a fixed environment. Wearable sensors use a single sensor or multiple sensors to collect acceleration and angular velocity data. Appropriate features are selected from these data, and the fall is classified using a specific algorithm. Bourke *et al.* used a triaxial accelerometer attached to a designed vest worn under clothing. They first detected the impact of the fall and concluded that a fall had occurred if the individual was lying down after the impact. Lai *et al.* [14] used a total of six triaxial accelerometers, respectively at the neck, hands, waist, and feet, to detect the fall and the injured areas. To improve the accuracy of fall detection, accelerometers with a gyroscope or a magnetometer are also utilized. Mao *et al*. developed a portable monitoring system using a cell phone and a triaxial accelerometer with a triaxial gyroscope and triaxial magnetometer [19]. In their system, once the fall was detected, the system would automatically connect to an emergency contact. Nari *et al*. used a triaxial accelerometer with a triaxial gyroscope and detected falls based on the threshold method [20]. Yang *et al*. have identified the fall hazard using a wearable IMU attached to the individual's ankle with gait abnormality score to identify the risk of fall [23].

Threshold algorithms and machine learning techniques are commonly used to detect falls with the collected data. In this method, a specific threshold value is set for acceleration and angular velocity. The algorithm then determines that a fall had occurred when the data collected from the sensor exceed the threshold. In machine learning methods, relevant features are extracted from the data collected as a first step. The features are then used as inputs for the machine learning algorithms. Although many threshold methods are efficient and popular algorithms, it is difficult to set threshold values, particularly for different fall types [24]. Aziz *et al.* [25] compared several established threshold methods with five different machine learning algorithms (logistic regression, decision tree, naïve Bayes, K-nearest neighbor, and support vector machine (SVM)). They reported that machine learning techniques showed better overall performance than threshold methods. However, machine learning techniques may not be suitable for energy-efficient wearable fall detection systems as such systems typically require high-performance computer processing units for fall detection in real time [26]. An energy-efficient fall detection algorithm with high accuracy is still to be developed for such wearable systems.

Recently, camera-based fall detection methods have been applied to classify the different types of falls as delivering information on the fall type to medical doctors or clinicians can expedite medical assistance [27]. These previous studies have shown that falls can be reliably and accurately detected using camera-based systems. However, few studies have focused on classifying the different types of falls with a wearable system. Aziz *et al.* [15] classified the different types of falls using single and multiple triaxial accelerometers with linear discriminant analysis. However, the overall performance in terms of classification was low even with multiple sensors.

In this study, we developed an energy-efficient temporal vector angle method to classify different types of falls with a wearable fall detection system that includes a low-performance microcontroller. Dony and Wesolkowski [28] showed that the RGB vector angle from an image can be used for edge detection instead of the Euclidean-distance-based method. We applied this method to temporal signals collected from the IMU sensor in our algorithm called the temporal signal angle measurement (TSAM) algorithm. This study was conducted with following objectives: 1) to discriminate the five most common types of fall using TSAM with a single wearable device, 2) to validate the algorithm at a lower sampling frequency to make our system more suitable for an energy-efficient fall detection wearable system, and 3) to compare the performance of TSAM with that of machine learning algorithms in classifying the types of fall.

II. MATERIALS AND METHODS

A. PARTICIPANTS

A total of seven volunteers were recruited for this study. The present study protocol was reviewed and approved by the Institutional Review Board of Seoul National University Hospital (IRB No. 1504-056-664). Written informed consent was submitted by all the volunteers. The body mass and height of each volunteer were measured using a body composition analyzer (InBody 520; InBody, Seoul, South Korea). The body mass was measured to the nearest 0.1 kg, and height was measured to the nearest 0.1 cm.

B. DATA COLLECTION

A wearable sensor was developed with a microcontroller (ATmega 168; Atmel, California, USA) and an IMU (MPU-6000; InvenSense, California, USA). MPU-6000 provided the triaxial acceleration and triaxial angular velocity. An image of the developed sensor is shown in Fig.1(A). The device was worn on the left chest of the subjects as shown in Fig.1(B), where the x-axis of acceleration is toward the superior direction, y-axis is toward the lateral direction, and z-axis is toward the posterior direction. Fig.1(C) represents the block diagram of the system. The width, height and weight of the system were 3.5cm, 2.5cm and 4.83g

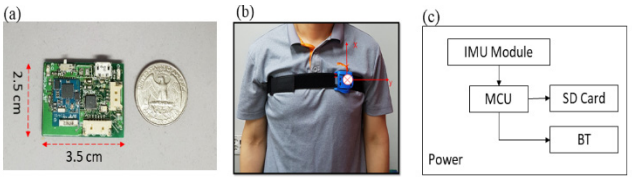

FIGURE 1. Pictures of (a) device printed circuit board and (b) location on left side of the chest during experiments. (c) block diagram of the device.

respectively. The 3.7 V with 470 mAh battery was used. The sampling frequency was set at 200Hz. The fall experiment was designed based on the five most common types of falls with respect to elderly adults in daily life; namely, incorrect weight shifting, trip or stumble, hit or bump, loss of support, and collapse [29]. Robinovitch *et al.* [29] have reported these fall types by observing 227 falls from 130 individuals at the long-term care facilities. The participants from this study watched the supplementary video of the previous studied for few times. After watching the video, the participants practiced each fall type for several times to get familiar with the protocol. Each fall type was performed nine times for each subject with three different falling speeds, fast, medium, and slow, for each type of fall.

C. TEMPORAL SIGNAL ANGLE MEASUREMENTS

The TSAM algorithm classifies measured signals into different types of falls by vectorizing temporal signals, both test and reference signals, and calculating the angle between the two different vectors. The calculated angle is referred to as an error, and the class with the smallest error between the test and reference signal is regarded as the answer. Before calculating the angle between the test and predefined reference signals, the test and reference signals were aligned using the following equations. After finding the time points that show the maximum changes in the test and reference signals using (1), the difference between the time points is calculated to obtain the shift index using (2).

$$\Delta f_j[t] = \frac{f_j[t+1] - f_j[t-1]}{2}$$

and

$$\Delta r_{ij}^k[t] = \frac{r_{ij}^k[t+1] - r_{ij}^k[t-1]}{2}, \tag{1}$$

where f is the test signal, r is the reference signal, j indicates the different types of signals collected from the IMU sensor (i.e. x-axis acceleration), i is the n$^{\text{th}}$ reference signal, and k represents the different fall types.

$$S_{ij}^k = \arg\max_t \left|\Delta f_j[t]\right| - \arg\max_t \left|\Delta r_{ij}^k[t]\right|, \tag{2}$$

where S is the shift index used to align the test and the reference signals. With the shift index and rectangular window, the test and reference signals are shifted and segmented to align the signals using (3).

$$f_j[t] = \begin{cases} f_j[t] \times rect\left[\dfrac{t - \left(\frac{l+S_{ij}^k}{2}\right)}{l - S_{ij}^k}\right], & S_{ij}^k \geq 0 \\ f_j[t] \times rect\left[\dfrac{t - \left(\frac{l-S_{ij}^k}{2}\right)}{l - S_{ij}^k}\right], & S_{ij}^k < 0, \end{cases}$$

and

$$r_{ij}^k[t] = \begin{cases} r_{ij}^k\left[t - S_{ij}^k\right] \times rect\left[\dfrac{t - \left(\frac{l+S_{ij}^k}{2}\right)}{l - S_{ij}^k}\right], & S_{ij}^k \geq 0 \\ r_{ij}^k\left[t - S_{ij}^k\right] \times rect\left[\dfrac{t - \left(\frac{l-S_{ij}^k}{2}\right)}{l - S_{ij}^k}\right], & S_{ij}^k < 0, \end{cases} \tag{3}$$

where f_j is shifted the test signal, and r_{ij}^k is the shifted reference signal.

Following signal alignments, the test and the references signal were vectorized using (4).

$$\overrightarrow{f_j} = (f_j[t_1], f_j[t_2], f_j[t_3], \cdots, f_j[t_{l-S_{ij}^k}]),$$

and

$$\overrightarrow{r_{ij}^k} = (r_{ij}^k[t_1], r_{ij}^k[t_2], r_{ij}^k[t_3], \cdots, r_{ij}^k[t_{l-S_{ij}^k}]) \tag{4}$$

The angles between the vectorized test signals and reference signals are then calculated using (5).

$$\theta_{ij}^k = \text{abs}(\cos^{-1}\frac{\overrightarrow{r_{ij}^k} \cdot \overrightarrow{f_j}}{\left\|r_{ij}^k\right\| \cdot \left\|f_{ij}\right\|}), \tag{5}$$

where θ is the absolute value of the angle between the test and reference signals.

The total error for each fall type is then obtained using (6), followed by fall classification using (7).

$$E^k = \sum_{i=1}^{N}\sum_{j=1}^{6}\theta_{ij}^k, \tag{6}$$

where E is the error for a specific fall type.

The fall type is determined by finding the fall type with the smallest error using (7).

$$\text{y} = \arg\min_k E^k, \tag{7}$$

where y is the final classified fall type. The block diagram and visualized process of the algorithm is shown in Fig 2.

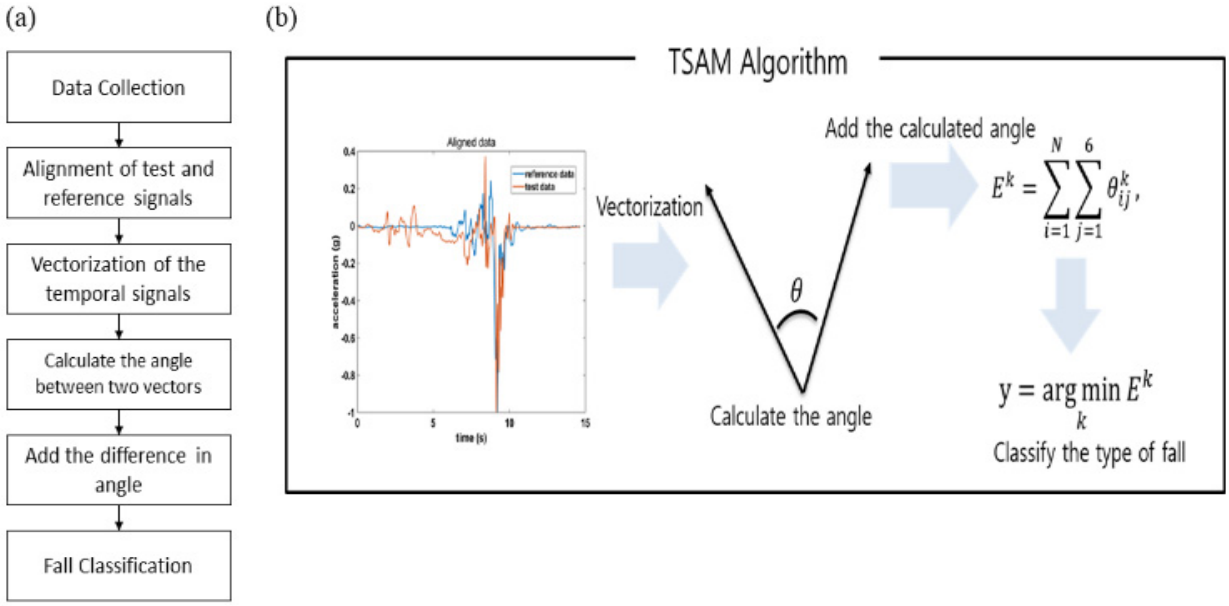

FIGURE 2. (a) Block diagram of the algorithm. (b) Visualization of the algorithm process.

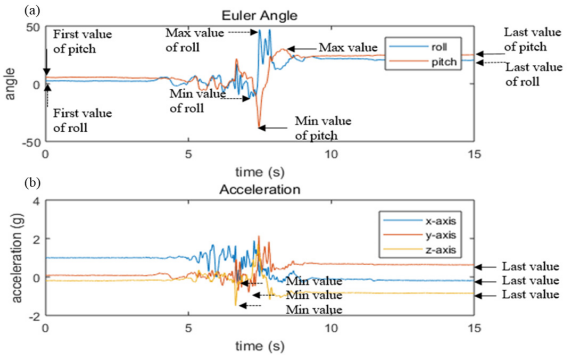

FIGURE 3. Feature extraction from IMU data. (a) Shows angular velocity in X and Y direction. Feature 1 through 10 were calculated by subtracting first and last value, first and maximum value, first and minimum value, last and maximum value, and last and minimum value of each X and Y direction. (b) Show the acceleration data in X, Y, and Z direction. Feature 11 was determined based on the order of last value as shown in (8). Feature 12 was determined based on the order of last value as shown in (9).

D. SIGNAL PROCESSING AND STATISTICAL ANALYSIS

All data analyses and classification were performed using MATLAB 2017a (MathWorks, Massachusetts). For the machine-learning-based classification, a total of 12 features were extracted from the data collected from the IMU sensor. Five features were obtained from the angular velocity, whereas two features were obtained from the acceleration data. The representative data of the angular velocity and acceleration are shown in Fig.3. Ten features were selected from the x- and y-axes of the angular velocity representing the differences between the first and last, first and maximum, first and minimum, last and maximum, and last and minimum values of the angular velocity. The feature selected from the acceleration data was decided based on the order of the last value of the acceleration on the x-, y- and z-axes. If the acceleration along the x-axis had the highest value followed by the y and z axes, the value of the feature was 1. The last feature was decided based on the order of the minimum value of the acceleration along the x-, y-, and z-axes. For example, if the x-axis had the smallest minimum value, the value of the feature was ''1''. The detailed definition of the two features is given in (8) and (9). After selecting the features, they were validated with the one-way analysis of variance (ANOVA) and t-test with the Bonferroni correction. The significance level of the p-value was 0.01 for the one-way ANOVA test and 0.005 for the t-test.

$$Feature\ 11 = \begin{cases} 1, & X > Y > Z \\ 2, & X > Z > Y \\ 3, & Y > X > Z \\ 4, & Y > Z > X \\ 5, & Z > X > Y \\ 6, & Z > Y > X \end{cases} \tag{8}$$

$$Feature\ 12 = \begin{cases} 1, & X > Y\ and\ Z \\ 2, & Y > X\ and\ Z \\ 3, & Z > X\ and\ Y \end{cases} \tag{9}$$

To classify the different types of falls, TSAM and three different machine learning algorithms, SVM, K-nearest neighbors (KNN), and random forest were used in this study, and their performance were compared. The three machine learning algorithms were selected because have been widely used and validated in various field [30]–[32]. A 10-fold cross-validation method was used to validate the model. For the machine learning algorithms, each class was randomly divided into 10 different subsamples: nine subsamples were used to train the model, and the remaining subsample was used for the validation. This process was repeated ten times,

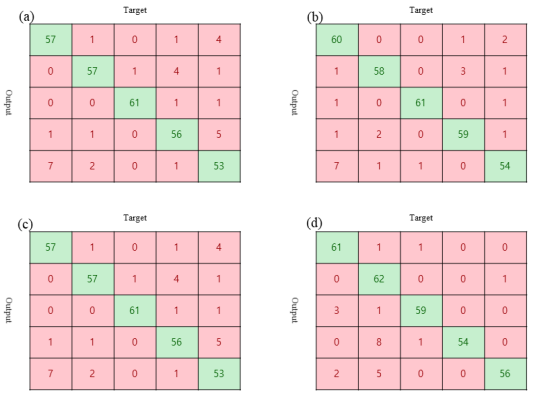

FIGURE 4. Result of 10-fold validation shown with confusion matrix for (a) support vector machine, (b) k-nearest neighbor, (c) random forest, and (d) temporal signal angle measurement.

excluding a different subsample on each occasion. On the other hand, for the TSAM algorithm, each of the nine subsamples was used as the reference signal, and the remaining subsample was used as the test signal. The errors between the test signal and each reference signal were calculated using (1)–(7). The mean value of the errors for each type of fall was then compared, and the fall type with the least error was determined as the fall type for the test signal. This process was repeated ten times for all test signals, excluding a different subsample each time. The cross-validated result was examined by comparing the accuracy, sensitivity, and specificity. The accuracy represents the proportion of true results, sensitivity represents the proportion of true positives from predicted positives, and specificity represents the proportion of true negatives from predicted negatives. The parameters were calculated using the (10), (11) and (12), as shown at the bottom of this page.

After classifying the different types of fall, the original data collected from the IMU sensor were downsampled into 100, 66.7, 50, 40, 30.3, 20, and 10 Hz signals. The alignment between the test and reference signals was performed using TSAM through the aforementioned process. Additionally, the features were extracted from the downsampled data for machine learning algorithms. The TSAM, SVM, KNN, and random forest methods were applied to classify the different types of falls, and their performances were compared.

III. RESULTS

All participants were male, and the mean age was 27.9 years. The mean weight was 74.5 kg, and the mean height was 174.7 cm. The mean and standard deviation of all the features are given in Table 1. The result of the one-way ANOVA test showed that all independent variables were significantly different among groups ($p < 0.01$). The result of the t-test with Bonferroni correction is given in Table 1. Where the features are significantly different ($p < 0.005$) between the fall types, it is also indicated in the table with a superscript. Among the 60 features for all five different types of falls, 26 features significantly differed for all four different fall types. In contrast, 16 features differed for three other fall types. Moreover, two features differed for two different fall types, and two features differed for one different fall type.

The confusion matrixes of all three machine learning algorithms and that for the TSAM algorithm are shown in Fig. 4. Fig. 5 shows the accuracy, sensitivity, and specificity of the cross-validated result of all four models at all frequencies ranging from 10 to 200 Hz. The accuracy for SVM ranged from 88.6% to 93.0%, whereas the accuracy for KNN ranged from 89.8% to 92.4%, and that for the random forest ranged from 90.5% to 92.8%. The accuracy for TSAM ranged from 91.8% to 93.3%. The sensitivity ranges for SVM, KNN, random forest, and TSAM were 88.6% to 93.7%, 85.7% to 92.4%, 90.5% to 92.7%, and 91.8% to 93.3%, respectively. The specificity for SVM ranged from 96.3% to 98.3%. The specificity for KNN ranged from 97.0% to 98.1%, and that for the random forest ranged from 97.6% to 98.2%. In contrast, the specificity for TSAM ranged from 97.9% to 98.3%.

IV. DISCUSSION

In this study, the five most common types of fall were successfully classified using a single wearable device with the TSAM and machine learning algorithms. Most of the previous studies focused solely on the detection of falls. Li *et al.* [2] developed a fall detection system using two accelerometers with a gyroscope located at the chest and right thigh to detect falls. Karantonis *et al.* [33] also detected falls using a triaxial accelerometer. In contrast, we classified the five most common fall types reported in previous studies [26]. Moreover, the algorithms were validated while downsampling the signals and still have shown an excellent performance. It has been reported that lower sampling frequency allows to scale down CPU speed, thus, reducing the power consumption [34]. As shown in Table 2, our study has performed at lowest sampling frequency among studies that used accelerometers or IMU sensors. All the classification models, in terms of accuracy, sensitivity, and specificity, showed excellent performance in discriminating the types of fall.

$$\text{Accuracy} = \frac{True\ Positive + True\ Negative}{True\ Positive + Ture\ Negative + False\ Positive + Flase\ Negative} \text{X100} \tag{10}$$

$$\text{Sensitivity} = \frac{True\ Positive}{True\ Positive + False\ Negative} X100 \tag{11}$$

$$\text{Specificity} = \frac{True\ Negative}{True\ Negative + False\ Positive} X100 \tag{12}$$

TABLE 1. Mean and standard deviations of independent variables.

Data Type	Feature Number	Feature	Type A	Type B	Type C	Type D	Type E	p-value
X-axis Angular Velocity	1	First - Last (Deg / Sec)	12.77(14.59)$^{2,}_{3,4}$	-20.50(6.34)^{1,4,5}	-21.34(5.90)^{1,4,5}	-9.73(8.01)^{1,2,3,5}	12.11(21.10)^{1,2,3,4}	<0.01
	2	First - Max (Deg / Sec)	-47.57(17.44)$^{2,}_{3,4,5}$	-23.66(8.93)^{1,3,5}	-55.26(15.51)^{1,2,4,5}	-22.36(12.84)^{1,3}	-32.09(9.15)^{1,2,3}	<0.01
	3	First - Min (Deg / Sec)	27.61(16.50)$^{2,}_{4,5}$	54.67(11.79)^{1,3,5}	32.19(7.29)^{1,2,4,5}	50.13(14.71)^{1,3,5}	23.76(15.21)^{1,2,3,4}	<0.01
	4	Last - Max (Deg / Sec)	-34.80(11.13)$^{2,}_{4}$	-44.16(10.81)^{1,3,5}	-76.60(17.52)^{2,4,5}	-32.09(11.70)^{1,3,5}	-19.98(24.58)^{2,3,4}	<0.01
	5	Last - Min (Deg / Sec)	31.83(12.58)$^{2,}_{3,4,5}$	9.46(13.01)^{1,3,4,5}	-5.32(12.26)^{1,2,4,5}	16.25(21.61)^{1,2,3,5}	22.34(12.95)^{1,2,3,4}	<0.01
Y-axis Angular Velocity	6	First - Last (Deg / Sec)	40.38(15.66)$^{2,}_{3,4,5}$	34.18(12.57)^{1,3,4,5}	10.85(10.71)^{1,2,4,5}	40.41(18.62)^{1,2,3,5}	35.87(12.22)^{1,2,3,4}	<0.01
	7	First - Max (Deg / Sec)	-45.35(17.85)$^{2,}_{4}$	-23.36(12.93)^{1,3,5}	-39.94(12.88)^{2,4}	-27.98(13.53)^{1,3,5}	-46.52(16.56)^{2,4}	<0.01
	8	First - Min (Deg / Sec)	20.96(14.55)$^{2,}_{3,4,5}$	33.98(11.37)^{1,4}	39.29(13.97)^{1,4}	59.87(18.26)^{1,2,3,5}	35.61(11.95)^{1,4}	<0.01
	9	Last - Max (Deg / Sec)	-13.52(8.87)^{3,5}	-13.90(10.36)^{3,5}	-45.26(18.08)^{1,2,4,5}	-11.73(10.80)^{3,5}	-24.18(16.43)^{1,2,3,4}	<0.01
	10	Last - Min (Deg / Sec)	52.79(12.74)$^{2,}_{3,4}$	43.44(11.69)^{1,3,4,5}	33.97(17.03)^{1,2,4,5}	76.13(25.49)^{1,2,3,5}	57.95(13.22)^{2,3,4}	<0.01
Acceleration	11	Order of Last value	2.75(0.67)^{2,3}	2.19(1.38)^{1,3}	3.67(1.47)^{1,2,4,5}	2.21(1.84)^{3}	2.46(0.89)^{3}	<0.01
	12	Order of Min Value	2.57(0.67)^{2,4}	2.02(0.22)^{1,3,4,5}	2.63(0.63)^{2,4}	1.78(0.46)^{1,2,3,5}	2.30(0.87)^{2,4}	<0.01

P-value on the very right side of the table is the result of one-way analysis of variance. Significance tests between classes were performed based on student t-test, followed by Bonferroni correction to find new alpha value ($P < 0.005$).
[1] Significantly different to type A; [2] Significantly different to type B; [3] Significantly different to type C; [4] Significantly different to type D; [5] Significantly different to type E;

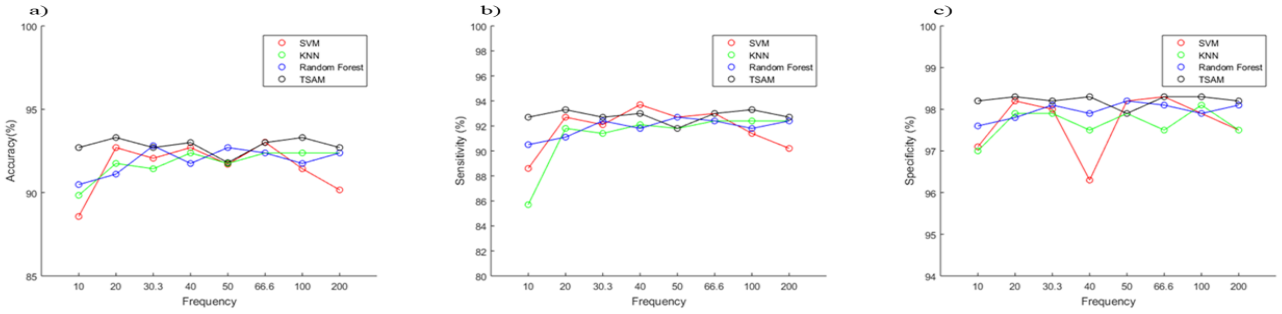

FIGURE 5. Change in (a) accuracy, (b) sensitivity, and (c) specificity of the classification models with frequency. The one versus all method was used to calculate the sensitivity and specificity.

Ghasemzadeh *et al.* [26] reported the five most common types of fall associated with the elderly through an observational study between April 2007 through June 2010. However, as summarized in Table 2, there are only a few studies related to the discrimination of common fall types. Aziz *et al.* compared the classification results of seven different fall types using a single to four accelerometers. They concluded that the combination of three sensors at the left ankle + right ankle + sternum provided the best performance [15]. However, it may be uncomfortable to wear multiple sensors at different parts of the body. We used only one sensor device in this study for classifying the types of fall. Also, their sensitivity was 83% and specificity was 89%, whereas our sensitivity and specificity were 93 and 98%.

In this study, we placed the sensor on the left side of the chest of the individuals instead of using a wrist-type device or a smart watch. The sensor position resulted in an improvement in the accuracy of the classification as the center of the body is located close to the chest. Additionally, the signal collected from the wrist varies widely depending on the type of fall and orientation of the arm [35]. Kangas *et al.* [13] compared different fall detection algorithms with acceleration signals acquired from the waist, head, and wrist. They concluded that the wrist is not an appropriate site for fall

TABLE 2. A table summarizing previous study for fall detection.

Author	Year	Sensor Type	Fall Type	Sampling Frequency	Feature	Algorithm	Performance
Miaou et al	2006	Omni-camera	Fall/Nonfall		The change in ratio of height and width from the silhouettes	Threshold algorithm	Accuracy: 81%
Parra-Dominguez et al	2015	Depth-camera	Fall and near fall	18.6 frames/s	Fourier coefficients and entropy metrics of instantaneous velocity	Random forest	Accuracy: 98%
Bian et al	2015	Depth-camera	Fall/Nonfall	30 frames/s	3-D trajectory of the head joint	Support vector machine	Accuracy: 98%
Rougier et al	2011	Depth-camera	Fall/Nonfall	30 frames/s	1. Human centroid height relative to the ground 2. Body velocity	Threshold algorithm	Accuracy: 99%
Yu et al.	2013	Traditional camera	Fall/Nonfall	5 frames/s	Extracted ellipses and shape-structure feature from the image	one-class support vector machine	True positive rate: 100 False negative rate: 3%
Kangas et al	2008	Three triaxial accelerometers	Fall/Nonfall	400 Hz	1. Total sum vector 2. Dynamic sum vector 3. Vertical acceleration 4. Falling index	Threshold algorithm	Accuracy: 98%
Lai et al	2011	Six triaxial accelerometers	1.Fall/Nonfall 2.Level of injury 3.Injured area		1. Sum vector magnitude 2. Activity single magnitude Area	Threshold algorithm	93%
Aziz et al	2014	four triaxial accelerometers	7 different types of all	128 Hz	Mean and variance in X, Y, and Z acceleration traces	Linear discriminant analysis algorithm	Sensitivity: 83% Specificity: 89%
Yang et al	2017	IMU sensor	Fall hazard-identification	128 Hz	1. Stride time 2. Stride distance 3. Average velocity 4. Maximum foot clearance 5. Stance ratio 6. Swing ratio	Gait abnormality score	NA
Mao et al	2017	IMU sensor	Fall/Nonfall	100 Hz	1. RMS of acceleration 2. Orientation of the user	Threshold detection	Accuracy: 100%
Nari et al	2016	IMU sensor	Fall/6 types of activities		1. Single vector magnitude 2. Angular velocity	Threshold detection	Sensitivity: 90% Specificity: 87%
Antwi_Afari et al	2018	Insole pressure system	Change in spatial foot regions and loss of balance events	50 Hz	1. Mean pressure 2. Peak pressure 3. Pressure-time integral 4. A/P COP 5. M/L COP	Observed statistical significance of the five features	NA

detection. Even though it might be possible to detect falls from the wrist, such as using the Apple Watch Series 4, we believe that the wrist may not be suitable for wearing devices used for detection of different fall types owing to its high dependency on the orientation of the arm.

There are limitations in this study. First of all, the number of subjects participated in the study was relatively small. Also, all experiments were performed in the laboratory setting. To further validate our algorithm, it needs to be tested with real fall data obtained from elderly with the larger sample number.

V. CONCLUSION

In summary, we successfully classified the most common fall types based on machine learning and TSAM algorithms. The four algorithms showed equivalent performances between 200 to 30.3 Hz. However, TSAM outperformed the machine learning algorithms between 20 to 10 Hz. All algorithms also showed satisfactory results even when they were down-sampled to lower sampling frequencies. Thus, these results have demonstrated that our methodology could be applied to the energy-efficient wearable device with a low sampling frequency to classify different types of fall. We believe that

our system could expedite medical assistance in emergency situations caused by falls by providing the necessary information to medical doctors or clinicians. For future study, it would be appropriate to validate the algorithm with actual fall data in real-time from elderly subjects. Also, the system could be improved by implementing the algorithm in the device and give an emergency alarm when it detects the fall in real-time. The temperature drift of a MEMS gyroscope may become a potential error source for long-term monitoring of elderly falls. Calibration for temperature drift errors may be needed for the long-term monitoring. The related work here remains as future studies.

ACKNOWLEDGMENT

The authors would like to thank all the participants

REFERENCES

[1] N. Noury, "A smart sensor for the remote follow up of activity and fall detection of the elderly," in *Proc. IEEE-EMBS 2nd Annu. Int. Special Topic Conf. Microtechnol. Med. Biol.*, May 2002, pp. 314–317.
[2] Q. Li, J. A. Stankovic, M. A. Hanson, A. T. Barth, J. Lach, and G. Zhou, "Accurate, fast fall detection using gyroscopes and accelerometer-derived posture information," in *Proc. 6th Int. Workshop Wearable Implant. Body Sensor Netw. Conf. (BSN)*, 2009, pp. 138–143.
[3] M. F. Antwi-Afari and H. Li, "Fall risk assessment of construction workers based on biomechanical gait stability parameters using wearable insole pressure system," *Adv. Eng. Inform.*, vol. 38, pp. 683–694, Oct. 2018.
[4] S.-G. Miaou, P.-H. Sung, and C.-Y. Huang, "A customized human fall detection system using omni-camera images and personal information," in *Proc. 1st Transdisciplinary Conf. Distrib. Diagnosis Home Healthcare (D2H2)*, Apr. 2006, pp. 39–42.
[5] Z.-P. Bian, J. Hou, L.-P. Chau, and N. Magnenat-Thalmann, "Fall detection based on body part tracking using a depth camera," *IEEE J. Biomed. Health Inform.*, vol. 19, no. 2, pp. 430–439, Mar. 2015.
[6] C. Rougier, E. Auvinet, J. Rousseau, M. Mignotte, and J. Meunier, "Fall detection from depth map video sequences," in *Proc. Int. Conf. Smart Homes Health Telematics*. Berlin, Germany: Springer, 2011, pp. 121–128.
[7] E. E. Stone and M. Skubic, "Fall detection in homes of older adults using the Microsoft Kinect," *IEEE J. Biomed. Health Inform.*, vol. 19, no. 1, pp. 290–301, Jan. 2015.
[8] R. Planinc and M. Kampel, "Introducing the use of depth data for fall detection," *Pers. Ubiquitous Comput.*, vol. 17, no. 6, pp. 1063–1072, 2013.
[9] M. Yu, Y. Yu, A. Rhuma, S. M. R. Naqvi, L. Wang, and J. A. Chambers, "An online one class support vector machine-based person-specific fall detection system for monitoring an elderly individual in a room environment," *IEEE J. Biomed. Health Informat.*, vol. 17, no. 6, pp. 1002–1014, Nov. 2013.
[10] D. Anderson, J. M. Keller, M. Skubic, X. Chen, and Z. He, "Recognizing falls from silhouettes," in *Proc. IEEE Int. Conf. Eng. Med. Biol. Soc.*, Aug./Sep. 2006, pp. 6388–6391.
[11] C. Rougier, J. Meunier, A. St-Arnaud, and J. Rousseau, "Robust video surveillance for fall detection based on human shape deformation," *IEEE Trans. Circuits Syst. Video Technol.*, vol. 21, no. 5, pp. 611–622, May 2011.
[12] G. S. Parra-Dominguez, J. Snoek, B. Taati, and A. Mihailidis, "Lower body motion analysis to detect falls and near falls on stairs," *Biomed. Eng. Lett.*, vol. 5, no. 2, pp. 98–108, 2015.
[13] M. Kangas, A. Konttila, P. Lindgren, I. Winblad, and T. Jämsä, "Comparison of low-complexity fall detection algorithms for body attached accelerometers," *Gait Posture*, vol. 28, no. 2, pp. 285–291, 2008.
[14] C.-F. Lai, S.-Y. Chang, H.-C. Chao, and Y.-M. Huang, "Detection of cognitive injured body region using multiple triaxial accelerometers for elderly falling," *IEEE Sensors J.*, vol. 11, no. 3, pp. 763–770, Mar. 2011.
[15] O. Aziz, E. J. Park, G. Mori, and S. N. Robinovitch, "Distinguishing the causes of falls in humans using an array of wearable tri-axial accelerometers," *Gait Posture*, vol. 39, no. 1, pp. 506–512, 2014.
[16] F. Bagalà *et al.*, "Evaluation of accelerometer-based fall detection algorithms on real-world falls," *PLoS ONE*, vol. 7, no. 5, 2012, Art. no. e37062.
[17] A. K. Bourke *et al.*, "Evaluation of waist-mounted tri-axial accelerometer based fall-detection algorithms during scripted and continuous unscripted activities," *J. Biomech.*, vol. 43, no. 15, pp. 3051–3057, 2010.
[18] M. Kangas, A. Konttila, I. Winblad, and T. Jamsa, "Determination of simple thresholds for accelerometry-based parameters for fall detection," in *Proc. IEEE 29th Annu. Int. Conf. Eng. Med. Biol. Soc. (EMBS)*, Aug. 2007, pp. 1367–1370.
[19] A. Mao, X. Ma, Y. He, and J. Luo, "Highly portable, sensor-based system for human fall monitoring," *Sensors*, vol. 17, no. 9, p. 2096, 2017.
[20] M. I. Nari, S. S. Suprapto, I. H. Kusumah, and W. Adiprawita, "A simple design of wearable device for fall detection with accelerometer and gyroscope," in *Proc. Int. Symp. Electron. Smart Devices (ISESD)*, Nov. 2016, pp. 88–91.
[21] B. Andò, S. Baglio, C. O. Lombardo, and V. Marletta, "A multisensor data-fusion approach for ADL and Fall classification," *IEEE Trans. Instrum. Meas.*, vol. 65, no. 9, pp. 1960–1967, Sep. 2016.
[22] G. Mastorakis and D. Makris, "Fall detection system using Kinect's infrared sensor," *J. Real-Time Image Process.*, vol. 9, no. 4, pp. 635–646, 2014.
[23] L. Yang, Y. Ren, H. Hu, and B. Tian, "New fast fall detection method based on spatio-temporal context tracking of head by using depth images," *Sensors*, vol. 15, no. 9, pp. 23004–23019, Sep. 2015.
[24] Y. S. Delahoz and M. A. Labrador, "Survey on fall detection and fall prevention using wearable and external sensors," *Sensors*, vol. 14, no. 10, pp. 19806–19842, 2014.
[25] O. Aziz, M. Musngi, E. J. Park, G. Mori, and S. N. Robinovitch, "A comparison of accuracy of fall detection algorithms (threshold-based vs. machine learning) using waist-mounted tri-axial accelerometer signals from a comprehensive set of falls and non-fall trials," *Med. Biol. Eng. Comput.*, vol. 55, no. 1, pp. 45–55, Jan. 2017.
[26] H. Ghasemzadeh, N. Amini, R. Saeedi, and M. Sarrafzadeh, "Power-aware computing in wearable sensor networks: An optimal feature selection," *IEEE Trans. Mobile Comput.*, vol. 14, no. 4, pp. 800–812, Apr. 2015.
[27] H. Foroughi, A. Naseri, A. Saberi, and H. S. Yazdi, "An eigenspace-based approach for human fall detection using integrated time motion image and neural network," in *Proc. 9th Int. Conf. Signal Process. (ICSP)*, Oct. 2008, pp. 1499–1503.
[28] R. D. Dony and S. Wesolkowski, "Edge detection on color images using RGB vector angles," in *Proc. IEEE Eng. Solutions Next Millennium, Can. Conf. Elect. Comput. Eng.*, vol. 2, May 1999, pp. 687–692.
[29] S. N. Robinovitch *et al.*, "Video capture of the circumstances of falls in elderly people residing in long-term care: An observational study," *Lancet*, vol. 381, no. 9860, pp. 47–54, 2013.
[30] L. Sheng, S. Qing, H. Wenjie, and C. Aize, "Diseases classification using support vector machine (SVM)," in *Proc. 9th Int. Conf. Neural Inf. Process. (ICONIP)*, vol. 2, Nov. 2002, p. 760–763.
[31] B. Toghiani-Rizi, C. Lind, M. Svensson, and M. Windmark. (2017). "Static gesture recognition using leap motion." [Online]. Available: https://arxiv.org/abs/1705.05884
[32] M. A. Shafique and E. Hato, "Classification of travel data with multiple sensor information using random forest," *Transp. Res. Procedia*, vol. 22, no. 22, pp. 144–153, Jan. 2017.
[33] D. M. Karantonis, M. R. Narayanan, M. Mathie, N. H. Lovell, and B. G. Celler, "Implementation of a real-time human movement classifier using a triaxial accelerometer for ambulatory monitoring," *IEEE Trans. Inf. Technol. Biomed.*, vol. 10, no. 1, pp. 156–167, Jan. 2006.
[34] W. R. Dieter, S. Datta, and W. K. Kai, "Power reduction by varying sampling rate," in *Proc. Int. Symp. Low Power Electron. Design*, 2005, pp. 227–232.
[35] K. Doughty, R. Lewis, and A. McIntosh, "The design of a practical and reliable fall detector for community and institutional telecare," *J. Telemed. Telecare*, vol. 6, no. 1, pp. 150–154, 2000.

SOON BIN KWON was born in Seoul, South Korea, in 1991. He received the B.S. degree from Boston University, Boston, MA, USA, in 2014. He is currently pursuing the integrated Ph.D. in bioengineering degree with Seoul National University. His main areas of research interests include signal classification algorithm and wearable systems.

JEONG-HO PARK was born in Pohang, South Korea, in 1992. He received the B.S. degree from the Kumoh National Institute of Technology, South Korea, in 2017, and the M.S. degree from the Daegu Gyeongbuk Institute of Science and Technology, South Korea, in 2019. He is currently with Hanwha Defense, South Korea. His main areas of research interests include signal classification algorithm, ultrasound systems, and ultrasound image segmentation.

CHIHEON KWON received the B.S. degree from the University of Ulsan, South Korea, in 2013, and the M.S. degree from Seoul National University, in 2015. He joined the Institute of Medical and Biological Engineering, South Korea, in 2016. His main areas of research interests include wearable systems and signal processing.

HYUNG JOONG KONG received the B.S. degree in electrical engineering and the M.S. and Ph.D. degrees in biomedical engineering from Seoul National University, Seoul, South Korea, in 2000, 2003, and 2009, respectively. From 2001 to 2009, he was a Research Member of the Department of Biomedical Engineering, Seoul National University Hospital (SNUH), Seoul, where the major research activities were the development of electronic instrumentation and intelligent algorithm for medical and biological applications, including telemedicine, telemetric urodynamic systems, electronic stethoscope, and retinal image analysis. From 2009 to 2012, he was a Postdoctoral Researcher with the Department of Anesthesiology and the Pain Medicine and the Department of Plastic and Reconstructive Surgery, SNUH, where he was a Research Assistant Professor with the Office of Hospital Information, from 2013 to 2016, where the major research interests were medical informatics and hospital information systems. He joined the Department of Biomedical Engineering, College of Medicine, Chugnam National University Hospital, as a Faculty Member, in 2016, where he is currently an Assistant Professor. He is a member of the Korea Society of Medical and Biological Engineering and the Korean Society of Medical Informatics.

JAE YOUN HWANG received the B.S. degree in electrical engineering from Korea University, Seoul, South Korea, in 2001, the M.S. degree in biomedical engineering from Seoul National University, Seoul, in 2003, and the Ph.D. degree in biomedical engineering from the University of Southern California, Los Angeles, CA, USA, in 2009.

He has been with the Faculty of the Department of Information and Communication Engineering, Daegu Gyeongbuk Institute of Science and Technology, Daegu, South Korea, where he is currently an Associate Professor. His current research interests include the development of a multimodality imaging system based on high-frequency ultrasound and optical techniques, and the development of novel mobile healthcare systems for the diagnosis of various diseases.

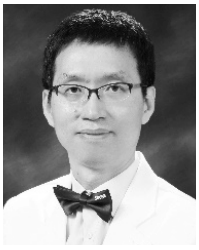

HEE CHAN KIM (M'95) received the Ph.D. degree in control and instrumentation engineering (biomedical engineering major) from Seoul National University, Seoul, South Korea, in 1989. From 1989 to 1991, he was a Staff Engineer with the Artificial Heart Research Laboratory, National Institute of Health, The University of Utah, Salt Lake City, USA, supported by the Electrohydraulic Total artificial Heart Project. He joined the Faculty of the Department of Biomedical Engineering, College of Medicine, Seoul National University, and Seoul National University Hospital, in 1991, where he is currently a Professor leading Medical Electronics Laboratory(MELab). His major research activities are in the MELab, which include the development of intelligent algorithms and electronic instrumentations for medical and biological applications, including artificial organs (such as artificial heart and artificial pancreas), biosensors, ubiquitous/mobile healthcare systems, and man-machine interface. He has published over 180 peer-reviewed scientific papers in international journals in his research areas. He holds over 170 patents. He is a member of the Korea Society of Medical and Biological Engineering, the IEEE/EMBS, and the American Society of Artificial Internal Organs.